Analyst

Hyper-Raman spectroscopy of biomolecules

Journal:	*Analyst*
Manuscript ID	AN-ART-04-2023-000641.R4
Article Type:	Paper
Date Submitted by the Author:	20-Nov-2023
Complete List of Authors:	Marble, Christopher; Texas A&M University, Biomedical Engineering Marble, Kassie; Texas A&M University, Biomedical Engineering Keene, Ethan; Texas A&M University, Biomedical Engineering Petrov, Georgi; Texas A&M University Yakovlev, Vladislav; Texas A&M University, Biomedical Engineering

ARTICLE

Hyper-Raman spectroscopy of biomolecules

Christopher B. Marble,*[a] Kassie S. Marble,[a] Ethan B. Keene,[b,c] Georgi I. Petrov,[b] and Vladislav V. Yakovlev [a,b,d]

Received 00th January 20xx,
Accepted 00th January 20xx

DOI: 10.1039/x0xx00000x

The hyper-Raman scattering (HRS) spectra of biologically significant molecules (D-glucose, L-alanine, L-arabinose, L-tartaric acid) in aqueous solutions are reported. The HRS spectra were measured using a picosecond laser at 532 nm operating at a MHz repetition rate. High signal to noise spectra were collected with a commercial spectrometer and CCD without resonant, nanoparticle, or surface enhancement. The HRS peak frequencies, relative intensities, band assignments, and depolarization ratios are examined. By comparing HRS to Raman scattering (RS) and infrared absorption spectra we verify that the IR-active vibrational modes of the target molecules are observed in HRS spectra but come with substantially different peak intensities. The HRS of the biomolecules as well as water, dimethyl sulfoxide, methanol, and ethanol were deposited into a data repository to support the development of theoretical descriptions of HRS for these molecules. Depositing the spectra in a repository also supports future dual detection RS, HRS microscopes which permit simultaneous high-spatial-resolution vibrational spectroscopy of IR-active and Raman-active vibrational modes.

1. Introduction

Vibrational spectroscopy techniques such as infrared absorption (IR) and Raman spectroscopy (RS) are well-established and are known to provide critical insights into the structures of complex molecules.[1-8] These complex molecules are traditionally investigated using a combination of IR and RS since their selection rules, which dictate what vibrations are detectable, are different. The IR selection rules reflect a change in the existing net dipole moment of the molecule during vibration while Raman selection rules reflect a change in the induced polarization (susceptibility) of the molecule during vibration. These responses are, in general, complementary to each other and collectively detect most simple molecular vibrations in organic molecules. While both IR and RS have advantages for specific applications, RS has become the dominant optical technique for probing chemical signatures in biological systems. The sensitivity of RS can be dramatically increased via techniques such as resonant Raman,[9,10] surface enhancement,[11] coherent anti-Stokes Raman scattering,[12-14] etc. These sensitivity enhancements have been found to even allow for the detection of individual molecules.[15-16] In contrast: (1) IR does not enjoy the same breath of enhancement techniques, (2) it suffers from extremely strong water librational bands under 1000 cm^{-1} leaving most of the fingerprint regime to be unmeasurable for molecules in aqueous solution,[17] and (3) the spatial resolution of IR microscopy is diffraction limited to the order of several microns. The disadvantages of IR spectroscopy, particularly when applied to studying aqueous samples, has caused researchers to neglect the Raman-silent transitions, essentially limiting our understanding of these biological systems. Other techniques to gain chemical information such as x-ray crystallography and NMR require extracting the sample from the Raman microscope which can be detrimental to tracking the time evolution of the sample. A new approach, one that allows simultaneous detection of Raman-silent modes with traditional RS, is necessary for us to obtain a large range of molecular vibrational information at the microscopic level.

Hyper-Raman spectroscopy (HRS) has recently gained attention as a promising new method to probe Raman silent vibrational modes.[18-29] HRS is a three-photon scattering process where two incident photons (ω_p) are annihilated and a single photon at a frequency $2\omega_p \pm \omega_v$ is generated, where ω_v is the frequency of the vibrational mode of the molecule.[29-33] HRS has distinct selection rules, but critically, all IR active modes are HRS active and, as such, HRS can provide complementary vibrational information to Raman spectroscopy (RS). Like RS, HRS enjoys many of the same enhancement techniques (resonant,[34,35] nanoparticle, surface enhancement),[36] while providing a better spatial resolution than RS. Most importantly, HRS can be performed simultaneously with Raman spectroscopy[22] allowing for the detection of IR-active and RS-active modes simultaneously with a single experimental setup. This can be done by simply splitting the scattered light by wavelength, via a dichroic mirror, to two spectrometers. HRS is a relatively

[a] Texas A&M University, Department of Physics and Astronomy, 4242 TAMU, College Station, TX 77843
[b] Texas A&M University, Department of Biomedical Engineering, 3120 TAMU, College Station, TX 77843.
[c] Tarleton State University, Department of Chemistry, Geosciences, and Physics, 1333 W. Washington Stephenville, TX 76402.
[d] Texas A&M University, Department of Electrical Engineering, 3127 TAMU, College Station, TX 77843.

† Electronic supplementary information (ESI) available: Data from validation of experimental design using pure DMSO, methanol, and ethanol with HRS spectra and depolarization ratios compared against existing literature. Other additional data including comparisons of HRS features against IR and Raman in literature and UV absorption cross-sections for the solutions studied. See DOI: 10.1039/x0xx00000x

unexplored analytical technique due to its dependence on the use of intense laser pulses without sacrificing the narrow laser linewidth condition, which has only recently become practical.[22] Other advantages of HRS include: (1) improved three-dimensional resolution similar in concept to two photon absorption as HRS intensity is dependent on square of the intensity of excitation intensity, (2) intensity-squared dependence allows for dramatically enhanced SNR when combined with surface enhancement (SEHRS), and (3) avoidance of one photon fluorescence.

As shown in this article, the HRS intensities of the water librational bands do not conceal the fingerprint spectra of other molecules in solution and the water spectra can be subtracted. This is a dramatic improvement in comparison to IR spectroscopy. Additionally, the water librations are easily quantified by HRS and provide insight into the "structure of water" which is elaborated on later in this article. Finally, while not shown in this article, there is interest in applying HRS to investigate highly symmetric molecules, as some so-called "silent modes," which are inactive in IR and Raman spectroscopy, can be observed. Most relevant for biological studies are the "silent" ring vibrations of aromatic structures like benzene recently characterized by HRS.[37]

The literature of HRS spectra for biologically important molecules includes measurements of water (H_2O) in liquid and solid phase,[38-40] aromatic amino acids,[41-42] BSA,[35] alcohols (methanol, ethanol, 1-propanol, and 2-propanol),[43] and benzene-h6, benzene-d6, and pyridine in the liquid phase.[37] This article investigates HRS spectroscopy of water and biomolecules in aqueous phase (D-glucose, L-alanine, L-arabinose, and L-tartaric acid) and provides relative intensities and depolarization ratios of the HRS spectra.

While the hyper Raman spectra of water has been previously reported,[38-40] we report and characterize the water spectra as it contributes to all of the following aqueous spectra. Additionally, the HRS signal of water was of interest to re-investigate since only the depolarization ratios for the OH stretch bands have been reported. In addition to the OH stretching region, we obtained spectra and depolarization ratios for librations and bend regions.

L-tartaric acid was then investigated due to its historical significance in discovering chirality and potential future use as a chiral molecule for demonstrating hyper-Raman optical activity.[44-47] As its optical properties have been thoroughly studied, it is an ideal molecule to use to test this system and contrast against its known IR and Raman spectra.[1]

All other molecules surveyed in this study are biological energy sources. For instance, L-alanine (a simple amino acid that constitutes of a high percentage of the amino acids in most proteins) is essential in linking carbohydrate and amino acid metabolism and providing energy to the central nervous system.[2,41] D-glucose is the primary energy source for all organisms.[5,47] L-arabinose (a monosaccharide constituent of many biopolymers in plant cell walls) regulates the blood glucose level and insulin resistance index via a unique property of reducing the absorption of sucrose in the small intestines.[5,48-50] Due to the relevance of these biological molecules as significant energy sources for various biosystems, we use them to showcase the capacity of HRS to obtain an extensive range of molecular vibrational information at the microscopic level.

Even though the HRS of both L-alanine and D-glucose have been previously investigated by C. Wen et. al, [41] and S. Maity et. al,[47] respectively, we report their spectra in this report for the following reasons. (1) While the hyper Raman signal of L-alanine has been previously reported, L-alanine's depolarization ratios have not been reported. (2). We report the hyper Raman signal of D-glucose in pure water for the first time, which is in good agreement with the spectra previously observed in IR and Raman spectroscopy. The previously reported HRS reported peaks (1616, 1540, 1351, 1230, and 1180 cm^{-1}) were inconsistent with IR and Raman spectra of the molecule.

Beyond providing the hyper-Raman spectrum, the relative HRS intensities (I_{HR}) and depolarization ratios $(\rho_{HR} = I_{HR\perp} / I_{HR||})$ are also provided for all molecules of interest. It should be noted that hyper-Raman depolarization ratios obey different rules than Raman depolarization ratios. In general, $0 \leq \rho_{HR} \leq 2/3$ and depolarized lines $(\rho_{HR} = 2/3)$ are HRS active but IR silent.[29] Similar to traditional Raman depolarization ratios, ρ_{HR} provides information about the symmetry of the molecule, and the vibrational mode represented by the HRS peak. For an example, see Ref. 9 where $\rho_{HR} = 0.2$ was seen as suggestive that only one nonzero element of the hyper-polarizability tensor contributed to their signal. The ρ_{HR} of the hyper-Rayleigh line is easier to measure than the ρ_R of the Rayleigh line as it is not contaminated with signal from scattered laser light from sources other than the target molecule. Furthermore, for a molecule with a known symmetry group deviations from the calculated $\rho_R$or ρ_{HR} provides insight into its interaction in solution often referred to as "symmetry breaking" behavior.[9]

Additional spectra and depolarization ratios of pure substances (methanol, ethanol, and dimethyl sulfoxide) are included in the supplement, where they were compared against existing HRS literature as a means of validating the existing setup.[20,43] Furthermore, as previously stated, this analysis demonstrates that the IR-active vibrational modes of these molecules in aqueous solution can be detected in the fingerprint regime where IR absorption spectroscopy is generally impractical.

2. Materials and Methods

Fig. 1 illustrates the hyper-Raman experiment, where a home-made high-power (> 6 W), high-repetition rate (0.5 - 30 MHz), mode-locked picosecond pulse (8 ps) laser was used as the excitation source. The design of this system has been described in prior publications.[20-22,25,26] Our samples were illuminated by focusing 532 nm laser pulses into quartz cuvettes using a 45 mm lens. As depicted in Fig. 1, the right-angle scattered light from the cuvettes was collected with an achromatic UV objective (Thorlabs, 20 ×, 0.4 NA) and imaged onto a HORIBA iHR 320 spectrometer using an achromatic UV lens. Spectra were recorded with a Symphony II, 2048 × 512 px UV-enhanced liquid-nitrogen cooled CCD. This CCD's resolution was found to be 0.05 nm full width at half maximum with the use of the fine

structure lines of mercury at 265 nm. It should also be noted that the system was calibrated using the emission lines of an Hg(Ar) lamp from 265 nm to 295 nm. The intensity calibration of the detector was verified by comparing the relative intensities of the mercury lines to the relative intensities reported by NIST (Ref. 51). Additional information about the spectrometer calibration and system resolution can be found in Refs. 25-26.

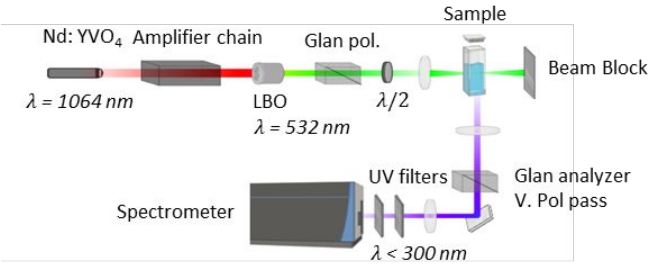

Fig 1. The right-angle HRS experiment.

The polarization of the emitted light was measured using a crossed Glan experiment, and a half wave plate was inserted between the Glan prisms to optimize polarization purity. The second Glan was then moved to the collection arm of the apparatus. The collection procedure was to take a series of measurements to record the hyper-Rayleigh and hyper-Raman emissions as a function of excitation polarization without moving the spectrometer grating. (1) This system was aligned to optimize the hyper-Rayleigh signal for parallel polarization and the hyper-Rayleigh line recorded. (2) The half wave plate was rotated 90 degrees by a computer-controlled mount and the hyper-Rayleigh signal for perpendicular polarization was recorded. (3) A 266 nm long pass filter was inserted, and steps 1 & 2 repeated to measure the parallel and perpendicular polarization hyper-Raman signals. As a check of optimized sample alignment, the hyper-Rayleigh signals were collected again (steps 5 & 6) after realigning the system to optimize signal for perpendicular polarization. In general, the difference in hyper-Rayleigh depolarization ratios was negligible between measurements. Pure liquids including dimethyl sulfoxide (DMSO) (Alfa Aesar #32434), ethanol (Sigma Aldrich #270741) and methanol (Millipore Sigma Uvasol #1.06002) were used as received. Deionized water (18.2MΩ cm) was used to dissolve ~50 % saturated aqueous solutions of D-glucose (2.5 M, Sigma #G8270), L-alanine (0.90 M, Sigma BioUltra #05129), L-arabinose (2.0 M, Sigma #A3256) and L-tartaric acid (5.0 M, Sigma-Aldrich #251380).

By rotating the half wave plate between V and H polarization, the polarized-HR spectra of these samples were measured, and the depolarization ratios calculated for each vibrational mode detected. The laser power introduced into the samples was between 1.5 – 1.7 W at repetition rates of 1.5 MHz and/or 3.0 MHz. An exposure time for one HRS measurement was generally 600 seconds and each spectrum shown is an average of 2 exposures. The collected spectra were then converted to wavenumbers, the background was subtracted, and the peaks were fitted using the MATLAB lsqcurvefit function. The uncertainty of our reported ρ_{HR} measurements ($\delta \rho_{Total}$) incorporate uncertainties in the reported fit ($\delta\rho_{Fit}$), estimated systematic uncertainty from the alignment ($\delta\rho_{Sys}$), and uncertainty from the total signal collected ($\delta\rho_{Count}$). In general, the uncertainty of the fit dominated the calculated total uncertainty which was calculated as: $\delta\rho^2_{Total} = \delta\rho^2_{Fit} + \delta\rho^2_{Sys} + \delta\rho^2_{Count}$.

3. Results and discussion

3.1 Water

The HRS spectra of H_2O (which has C_{2v} point group symmetry with a total of 9 molecular vibrational modes divided into symmetries a_1, a_2, b_1, b_2 respectively) compared favourably with the HRS spectra reported in literature[42-44] with two strong, broad librational modes, a bend, and multiple stretch modes (fit as three modes) shown in Fig. 2 and summarized in Table 1. Additionally, as seen in Korepanov et al.[39] for water, as well as a lesser extent for other hydrogen bonding (H-bonding) pure liquids such as methanol and ethanol, a broad quadratic background HRS response was observed for water. This broadband response was subtracted by the method reported in Ref. 26 and is not shown in the spectra below. Notably, the HRS intensities of the librational modes is of the same order of magnitude as the stretch modes unlike in Raman where the librations are extremely weak and often concealed in the solution background or in IR absorption where the librations are so strong that they are difficult to quantify and completely conceal the far-IR absorption spectra of other molecules in solution. The intermediate intensity of the HRS signal from librational modes has made hyper-Raman spectroscopy valuable for studying the temporary, semi-rigid, self-bonding networks formed by water in solution sometimes referred to as the "structure of water." HRS has been used to probe how the structure of water is modified by the addition of DMSO providing insight into the hydration shell dynamics of water in contact with organic molecules with polar functional groups. In the case of the DMSO-water system, the addition of DMSO dramatically modified the structure of water with blueshift/redshift of the 500/750 cm^{-1} water librations similar to the addition of large, negative salt ions like iodine.[26]

A single band fit of the OH stretch response was recently reported by Inoue et al.[40] In addition to a three-band fit of the OH stretching region, we obtained spectra and depolarization ratios for librations and bend regions. In the polarization dependent data reported in Fig. 2, we observe that the depolarization ratio of the two librational modes were dramatically different (0.60 +/- 0.03 versus 0.33 +/- 0.01). The calculated depolarization ratios for the three-band fit were computed. The OH stretching bands at 3330 cm^{-1} and 3594 cm^{-1} agreed with the value that Inoue et al.[40] obtained with their one-band fit (~ 0.18). However, the depolarization ratio of our third band around 3458 cm^{-1} (~ 0.3) was not in good agreement.

Polarized HRS detection combined with knowledge of the depolarization ratios of the two modes would allow for improved deconvolution of the two features. Improved deconvolution will play a valuable role in future studies of the modification of the structure of water in mixed liquid solutions

where tracking the evolution of the water librations into mixed liquid librations is complicated by the fingerprint vibrational spectra of the other liquid in solution.[26]

Table 1. Peak assignments for water with relative intensities (to the hyper-Rayleigh line) and depolarization ratios.

HRS (cm^{-1})*	Band Assignment	I_{Ratio} (x1000)	ρ
0	Hyper-Rayleigh	1000 +/- 45	0.21 +/- 0.02
503 +/- 6	Libration	27.3 +/- 1.6	0.60 +/- 0.03
748 +/- 5	Libration	48.7 +/- 2.7	0.33 +/- 0.01
1653	O-H Bend	8.2 +/- 0.4	0.37 +/- 0.01
3330	O-H Stretch	69.6 +/- 3.2	0.200 +/- 0.008
3458	O-H Stretch	36.1 +/- 1.7	0.30 +/- 0.02
3594	O-H Stretch	16.9 +/- 0.8	0.20 +/- 0.01

*Where the uncertainty is unstated, it is +/- 1 cm^{-1}.

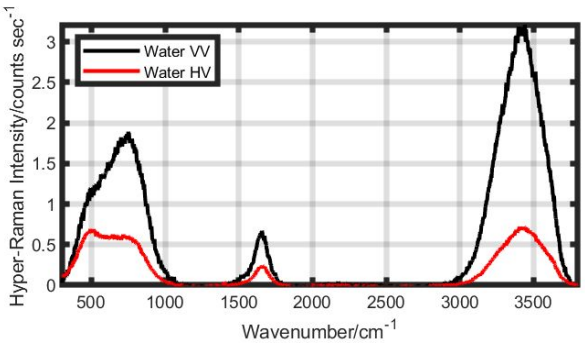

Fig. 2 The hyper-Raman spectra of deionized water for the VV and HV geometry are shown in black and red respectively post Savitzky-Golay filtering.

3.2 D-Glucose

Extensive work has been done towards chemically characterizing carbohydrates; including a recent publication on the HRS spectra of glucose.[47] However, that study did not attempt polarization resolved measurements and so the depolarization ratio of the vibrational modes were not reported. D-Glucose is known to have C_1 point group symmetry and has 66 internal vibrational modes with 6 external vibrations) with only symmetry species e. As such, all vibrations are active in both infrared and Raman spectra.[52] We summarize the HRS band assignments and report the depolarization ratio for glucose (as can be seen in Table 2). The high-wavenumber region of the HRS spectra of glucose was shown to contain the typical OH stretches (3520 and 3230 cm^{-1}) and CH stretches of CH_2/CH groups (2950, 2940, and 2890 cm^{-1}) seen in previous FTIR and Raman studies.[6] An additional peak was observed around 1638 cm^{-1} which was not identified in previous works (IR or Raman). We attribute this band to an enhanced, redshifted OH bend of water molecules H-bonding with the hydroxyl groups on the glucose molecule. This peak is excluded from the reported spectra in Fig. 3.

By comparing spectra of D-glucose and water (taken under identical conditions) we observe that the 1638 cm^{-1} response was dramatically enhanced in glucose compared to the other water bands (Fig. 3). This band's intensity ratio being significantly larger than all other bands observed in glucose (except for the hyper Rayleigh line). The high molar concentration of D-glucose (2.5 M) most likely distorted the OH bend mode by modifying the hydrogen bonding structure of H_2O in solution. This was unsurprising as the OH bend mode is known to be strongly sensitive to temperature fluctuations[22] and the addition of molecules that ionically bond or H-bond with water.[17] Likewise, the OH stretch modes of D-glucose were convoluted with the enhanced OH stretch of water.

The torsion vibration was seen in the HRS spectra; however, it appears as a broad feature centered around 1248 cm^{-1}. Bands at 1110, 1076, and 1037 cm^{-1} were characterized as C-O/C-C stretching modes and COH in-plane bending modes while the bands at 903 and 522 cm^{-1} were assigned to ring deformation and deformation modes. Measurement of the 1037 cm^{-1} band was the most import observation for this molecule as this band has been used to quantify glucose concentrations in blood and plasma via IR absorption spectroscopy.[6] In the polarization dependent data reported in Fig. 3, we observe that most of the depolarization ratios of the vibrational modes were all similar in value; except for the significant difference between the C-H symmetrical stretching modes (0.16 +/- 0.05 versus 0.31 +/- 0.04).

Table 2. Peak assignments for D-glucose with relative intensities (to the hyper-Rayleigh line) and depolarization ratios.

HRS (cm^{-1})*	Band Assignment	I_{Ratio} (x1000)	ρ
0	Hyper-Rayleigh	1000 ± 36	0.18 ± 0.02
522	$\beta_{ip}(CCC)$,$\beta_{ip}(CCO)$, $\beta_{ip}(OCO)$	0.88 ± 0.05	0.34 ± 0.03
903 +/- 2	$\beta_{ip}(CCH)$,$\beta_{ip}(CCO)$	1.00 ± 0.06	0.29 ± 0.03
1037	$\nu(CC)$,$\nu(CO)$, $\beta_{ip}(COH)$	3.5 ± 0.2	0.19 ± 0.02
1076	$\nu(CC)$,$\nu(CO)$, $\beta_{ip}(COH)$	0.50 ± 0.08	0.19 ± 0.05
1110 +/- 2	$\nu(CC)$,$\nu(CO)$, $\beta_{ip}(COH)$	5.1 ± 0.3	0.21 ± 0.02
1248 +/- 2	$\tau(CH_2)$	6.5 ± 0.4	0.34 ± 0.03
1322 +/- 3	$\omega(CH_2)$	3.0 ± 0.2	0.31 ± 0.03
1386 +/- 2	$\omega(CH_2)$	6.0 ± 0.4	0.31 ± 0.03
1449 +/- 3	$\delta(CH_2)$	4.4 ± 0.3	0.27 ± 0.03
2890 (est.)	$\nu_{sym}(CH_2)$	6.9 ± 0.8	0.26 ± 0.04
2940 (est.)	$\nu_{Sym}(CH_2)$	0.26 ± 0.04	0.16 ± 0.05
2950 (est.)	$\nu(CH)$	7.7 ± 0.1	0.31 ± 0.04
3230 (est.)	$\nu(OH)$	OH Overlap	0.45 (est.)
3520 (est.)	$\nu(OH)$	OH Overlap	0.42 (est.)

*Where the uncertainty is unstated, it is +/- 1 cm^{-1}.

Abbreviations: sym, symmetric; ip, in-plane; ρ, scissoring; ν,

stretching; τ, twisting; β, bending; OH Overlap, Overlap with water OH prevents estimate of bond intensity

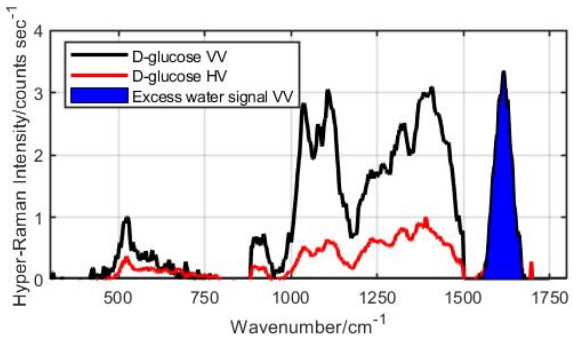

Fig. 3 The hyper-Raman spectra of D-glucose for the VV and HV geometry are shown in black and red respectively post Savitzky-Golay filtering and water subtraction. See supplement for spectra from 300 cm^{-1} to 3800 cm^{-1}.

3.3 L-Arabinose

The carbohydrate L-arabinose shares many bands with D-glucose as it also has a C_1 point group symmetry and is known to have 60 internal vibrational modes as well as 6 external modes with only one symmetry species e.[6] This is seen in the similarity of the two molecules HRS spectra (Fig. 4 and Fig. 3 respectively). These include broad H-bonded OH stretches (3600 cm^{-1} to 3100 cm^{-1}), CH stretches of CH_2/CH groups (3005, 2976, 2953, 2929, and 2887 cm^{-1}), and an arabinose-enhanced water OH bend centered around 1650 cm^{-1}. However, unlike D-glucose, L-arabinose has more observable low frequency features, as shown in Table 3. The most intense bands of L-arabinose were observed at 1094, 2887, and 2929 cm^{-1}, as shown by the intensity ratios in Table 3. These values contrast the prominent bands observed via Raman and IR.[6] For instance, one of the intense, Raman active bands was the 843 cm^{-1} band, a combination of CO ring stretching, CC ring stretching, and CO stretching vibrations which in the case of HRS is extremely weak. The IR active 1048 cm^{-1} band is also intense in the HRS spectrum, exhibiting the dominant contribution of the stretching modes of the endo and exocyclic CO groups. In particular, we see that fingerprint bands less than 872 cm^{-1} were all relatively weak even at high glucose concentrations in solution, for which depolarization ratios could not be calculated even after subtracting out the O-H librational background. Most significant for chemical identification were the identifications of the 1259 cm^{-1}, 1004 cm^{-1} and 612 cm^{-1} bands. The 1259 cm^{-1} band is characteristic of carbohydrates and the 1004 cm^{-1} and 612 cm^{-1} bands are unique markers that distinguish arabinose from other carbohydrates.[6]

Table 3. Peak assignments for L-arabinose with relative intensities (to the hyper-Rayleigh line) and depolarization ratios.

HRS (cm^{-1})*	Band Assignment	I_{Ratio} (x1000)	ρ
0	Hyper-Rayleigh	1000 ± 24	0.18 ± 0.01
382 (est.)	$\tau(OH)$	Very Weak	Unknown
510 (est.)	$\beta_{ip}(CCC)$, ring def	Very Weak	Unknown
577 (est.)	$\beta_{ip}(CCC)$, ring def	Very Weak	Unknown
612 (est.)	$\beta_{ip}(OCO)$	Very Weak	Unknown
645 (est.)	$\beta_{ip}(OCO)$	Very Weak	Unknown
700 (est.)	$\beta_{ip}(OCO)$	Very Weak	Unknown
872	$\beta_{ip}(CH)$	0.41 ± 0.02	0.60 ± 0.03
919	$\beta_{ip}(CCH)$	0.34 ± 0.02	0.47 ± 0.03
944	$\beta_{ip}(OCH)$	0.31 ± 0.02	0.28 ± 0.02
1004	$\nu_{as}(COC)$,$\nu(CC)$, $\beta_{ip}(CCH)$	1.66 ± 0.08	0.133 ± 0.007
1062 +/- 3	$\nu(CO)$, $\nu(CC)$, $\beta_{ip}(COH)$	1.2 ± 0.1	0.15 ± 0.03
1094	$\nu(CO)$	5.21 ± 0.26	0.17 ± 0.01
1145	$\nu(C-C)$	1.60 ± 0.08	0.20 ± 0.02
1219	$\tau(\mathrm{CH_2})$	1.63 ± 0.07	0.26 ± 0.01
1259	$\tau(\mathrm{CH_2})$	2.9 ± 0.2	0.35 ± 0.02
1307 (est.)	$\omega(\mathrm{CH_2})$	2.04 ± 0.12	0.25 ± 0.02
1345 (est.)	$\omega(\mathrm{CH_2})$	2.13 ± 0.11	0.26 ± 0.02
1373 (est.)	$\omega(\mathrm{CH_2})$	0.78 ± 0.09	0.27 ± 0.05
1400 (est.)	$\omega(\mathrm{CH_2})$	2.7 ± 0.2	0.21 ± 0.02
1450 (est.)	$\delta(CH_2)$	2.9 ± 0.2	0.24 ± 0.02
2887	$\nu_{sym}(CH_2)$	6.8 ± 0.5	0.22 ± 0.02
2929	$\nu(CH)$	10.3 ± 0.6	0.21 ± 0.02
2953	$\nu(CH)$	1.1 ± 0.3	0.18 ± 0.09
2976	$\nu_{as}(CH)$	3.2 ± 0.2	0.25 ± 0.02
3005	$\nu_{as}(CH_2)$	1.9 ± 0.2	0.29 ± 0.05
3100-3600 (est.)	$\nu(OH)$	OH Overlap	OH Overlap

*Where the uncertainty is unstated, it is +/- 1 cm^{-1}.

Abbreviations: sym, symmetric; as, asymmetric; ip, in-plane; ν, stretching; τ, twisting; ω, wagging; δ, scissoring; β, bending; ring def, ring deformation; OH Overlap, Overlap with water OH prevents estimate of bond intensity

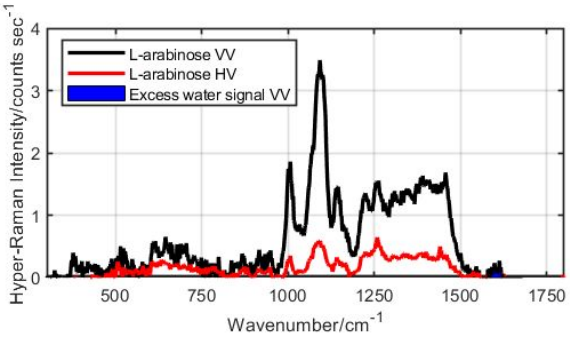

Fig. 4 The hyper-Raman spectra of L-arabinose for the VV and HV geometry are shown in black and red respectively post Savitzky-Golay filtering. See supplement for spectra from 300 cm^{-1} to 3800 cm^{-1}.

3.4 L-Alanine

The spectra of L-alanine was characterized by HRS[41] with the following bands observed: stretching modes, bending modes, rocking modes, and combinations of multiple modes (see Fig. 5 and Table 4). L-Alanine, like D-Glucose, has C_1 point group symmetry and is known to have 66 internal vibrational modes (with symmetry species 33 a_g and 33 a_u) as well as 6 translational (with the symmetry species 3 a_u and 3 a_g) and 6 rotational modes (with the symmetry species 3 a_u and 3 a_g).[53] The lowest frequency peak, excluding the solution OH librations, was centered around 541 cm^{-1}. This peak correlates with the OH bending band of L-alanine observed in both the Raman and IR spectra. These bands include the NH_3 puckering vibrational modes that appear around 1531 cm^{-1} and 1850 cm^{-1} with an additional mode assigned to the COO stretching and NH bending motions.[2,4] Like D-glucose, the high molar concentration of L-alanine used to collect HRS spectra (0.9 M) most likely distorted the OH bend mode resulting in an excess water signal around 1640 cm^{-1}.

Table 4. Peak assignments for L-alanine with relative intensities (to the hyper-Rayleigh line) and depolarization ratios.

HRS (cm^{-1})*	Band Assignment	I_{Ratio} (x1000)	ρ
0	Hyper-Rayleigh	1000 ± 20	0.18 ± 0.01
541	$r(COO^-), \nu(CC), \delta(CCN), \nu(CN)$	0.55 ± 0.02	0.63 ± 0.06
648	$\delta(COO^-), \delta(CCN), \nu(CC), r(COO^-)$	1.27 ± 0.06	0.34 ± 0.03
777	$\omega(COO^-), \delta(CCC)$	1.24 ± 0.05	0.27 ± 0.02
847	$\delta(COO^-), \upsilon_s(COO^-), \nu(\mathrm{C-C}), \nu(\mathrm{CN})$	0.54 ± 0.02	0.24 ± 0.02
920	$\nu(\mathrm{CN}), r(CH_3), \nu(\mathrm{CC})$	0.334 ± 0.009	0.32 ± 0.02
1005	$\nu(\mathrm{CC}), r(CH_3)$	0.38 ± 0.02	0.36 ± 0.03
1112	$r(NH_3^+)$	0.43 ± 0.02	0.17 ± 0.01
1142 +/- 2	$\nu_{as}(\mathrm{CCN}), r(CCN)$	0.193 ± 0.007	0.30 ± 0.02
1304	$\nu_{sym}(\mathrm{CCO}^-), r_{ip}(NH_3^+), r(CH)$	0.40 ± 0.01	0.14 ± 0.01
1353	$\delta(CH_3), \delta(NH_3^+)$	0.63 ± 0.03	0.34 ± 0.02
1379	$\delta_{as}(CH_3), \upsilon_{sym}(COO^-)$	0.078 ± 0.02	0.38 ± 0.02
1413	$\upsilon_{sym}(COO^-), \upsilon(CC), \delta_{as}(CH_3)$	2.60 ± 0.06	0.23 ± 0.01
1462	$\delta_{as}(CH_3)$	0.89 ± 0.05	0.23 ± 0.02
1530	$\delta_{sym}(NH_3)$	Not Detected	Unknown
2747 (est.)	$rp(CH_3)$	0.14 ± 0.02	0.17 ± 0.06
2899	$\nu(\mathrm{CH_3})$	0.20 ± 0.03	0.27 ± 0.06
2950	$\nu(CH_3)$	0.62 ± 0.03	0.25 ± 0.02
2984	$\nu(CH_3)$,	0.43 ± 0.03	0.32 ± 0.03
3007	$\nu(NH_3)$	0.29 ± 0.02	0.15 ± 0.02
3093 +/- 7	$\nu_{as}(NH_3)$	8.2 ± 0.3	0.24 ± 0.02

*Where the uncertainty is unstated, it is +/- 1 cm^{-1}.

Abbreviations: sym, symmetry; as, asymmetric; ip, in-plane; δ, scissoring; ν, stretching; τ, twisting; ω, wagging; r, rocking; rp, ring puckering

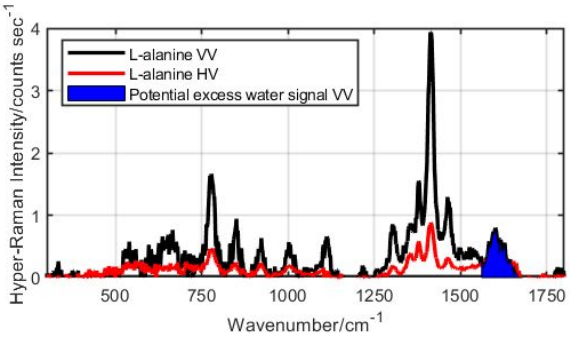

Fig. 5 The hyper-Raman spectra of L-alanine for the VV and HV geometry are shown in black and red respectively post Savitzky-Golay filtering. See supplement for spectra from 300 cm-1 to 3800 cm^{-1}.

3.5 L-Tartaric Acid

While L-tartaric acid (TA) has two chiral centers and belongs to the C_2 point group (low symmetry group), not all of the observed vibrational modes were all IR, Raman, and HRS active (see the supplemental material).[1] TA is known to have 90 internal vibrational modes (with symmetry species 46 a and 44 b) as well as 3 translational (with symmetry species a and 2b) and 3 rotational modes (with symmetry species a and 2b).[1,54] The hyper Raman spectra of L-tartaric acid was characterized by three COOH torsion vibrations (522 cm^{-1} – 686 cm^{-1}), two OCO angle deformations (778 cm^{-1} – 831 cm^{-1}), three C-C stretching modes (894 cm^{-1} – 992 cm^{-1}), two CHOH stretching modes (1089 cm^{-1} – 1136 cm^{-1}), three bending modes (1216 cm^{-1} – 1328 cm^{-1}), a COH angle deformation mode (1400 cm^{-1}), a broad C=O stretching mode (1730 cm^{-1}), a C-H stretching mode (2935 cm^{-1}), and two O-H stretching modes (3230 cm^{-1} and 3540 cm^{-1}). The spectra to 1800 cm^{-1} is shown as Fig. 6 and the analysis in Table 5. It should be noted that the three C-H bending modes observed between 1216 cm^{-1} and 1328 cm^{-1} were significantly more intense than the bands seen in the IR or Raman.[1] When compared to the HRS of water (as seen in Fig S7) this broad band can be separated into two peaks: (1) one shoulder peak around 3230 cm^{-1} which we believe corresponds to the stretching of O-H bonds characteristic in alcohol groups, (2) the other appearing to be an enhanced water stretching mode centered around 3540 cm^{-1}. Like D-glucose, the high molar concentration of L-alanine used to collect HRS spectra (5.0 M) most likely distorted the OH bend mode resulting in an excess water signal around 1640 cm^{-1}. The observation of the 1400 cm^{-1} band was an interesting observation for this molecule since this band has been used as a suitable biomarker compound for wine in archaeological residues.[55]

Table 5. Peak assignments for L-tartaric acid with relative intensities (to the hyper-Rayleigh line) and depolarization ratios.

HRS (cm^{-1})*	Assignment	I_{Ratio} (x1000)	ρ
0	Hyper-Rayleigh	1000 ± 30	0.22 ± 0.02
522	$\tau(COOH)$	3.2 ± 0.2	0.28 ± 0.03
595	$\tau(COOH)$	10.1 ± 0.5	0.21 ± 0.02
686	$\tau(COOH)$	1.9 ± 0.1	0.25 ± 0.03
778	γ (OCO)	1.28 ± 0.07	0.38 ± 0.04
831	γ (OCO)	4.5 ± 0.2	0.25 ± 0.02
894	$\nu(C-C)$	3.0 ± 0.1	0.27 ± 0.03
955	$\nu(C-C)$	0.43 ± 0.02	0.36 ± 0.04
992	$\nu(C-C)$	0.59 ± 0.03	0.35 ± 0.04
1089	$\nu(CHOH)$	2.2 ± 0.1	0.23 ± 0.02
1136	$\nu(CHOH)$	2.2 ± 0.1	0.20 ± 0.02
1216 +/-2	$\beta(CH)$	4.5 ± 0.3	0.30 ± 0.04
1274 +/- 2	$\beta(CH)$	14.6 ± 08	0.30 ± 0.03
1328	$\beta(CH)$	7.6 ± 0.5	0.32 ± 0.04
1400 +/-2	$\gamma(COH)$	6.2 ± 0.3	0.33 ± 0.04
1459 +/-2	$\nu(C-O)$	3.0 ± 0.2	0.32 ± 0.04
1730 +/- 2	$\nu(C=O)$	19 ± 1	0.34 ± 0.04
2935	$\nu(C-H)$	9.3 ± 0.6	0.32 ± 0.04
3230 (est.)	$\nu(O-H)$	5.3 (est.)	0.38 (est.)
3540 (est.)	$\nu(O-H)$	8.1 (est.)	0.17 (est.)

*Where the uncertainty is unstated, it is +/- 1 cm^{-1}.

Abbreviations: ν, stretching; τ, twisting; β, bending; γ, angle deformation

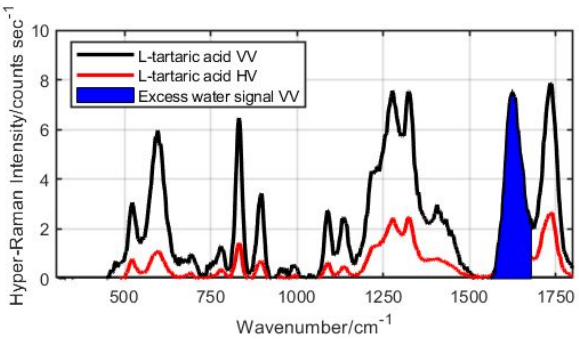

Fig. 6 The hyper-Raman spectra of L-tartaric acid for the VV and HV geometry are shown in black and red respectively post Savitzky-Golay filtering. See supplement for spectra from 300 cm^{-1} to 3800 cm^{-1}.

Conclusions

HRS measurements were performed on deionized water and concentrated aqueous solutions of D-glucose, L-alanine, L-arabinose, and L-tartaric acid. Reasonable detection times were achieved without resonant, surface, or nanoparticle enhancement and depolarization ratio values for vibrational modes with low SNR over the water background were reported. The methods used were validated against pure solutions of DMSO, methanol and ethanol whose values have been reported by other groups. The distinct depolarization ratios of the water librations may prove to be valuable in future efforts to study the structure of water as well as in subtracting the librations for analysing Raman silent modes in the fingerprint regime of molecules in aqueous solution. While the HR bands of H_2O were subtracted in each of the spectra, a residual feature (indicated by blue shaded areas in Figs. 3-6) remained in the HR spectra of these biomolecules. We believe this was due to the high molarity solutes modifying the hydrogen bonding structure of H_2O in solution. Long duration measurements with lower concentration samples could improve data quality. We observe the general trend for all molecules that HRS spectra tend to follow the selection rules of IR absorption spectroscopy, but display dramatically different band intensities. To achieve rapid detection at mMol concentrations signal enhancement techniques traditionally applied to Raman spectroscopy will need to be utilized.

Author Contributions

C. Marble: Formal analysis (lead)/Methodology (equal)/Validation (equal)/Investigation (equal)/Writing – original draft (equal)/Writing – review & editing (supporting); **K. Marble:** Formal analysis (supporting)/Validation (equal)/Writing – original draft (equal)/Writing -review & editing (supporting); **E. Keene:** Formal analysis (supporting)/Writing -review & editing (supporting); **G. Petrov:** Methodology (equal)/Validation (equal)/Investigation (equal); **V. Yakovlev:** Conceptualization (lead)/Formal analysis (supporting)/Funding acquisition (lead)/Investigation (equal)/Methodology (equal)/Supervision (lead)/Visualization (lead)/Writing – original draft (supporting)/Writing – review & editing (lead)

Conflicts of interest

There are no conflicts to declare.

Data Availability

Electronic supplementary information (ESI) available: Data from validation of experimental design using pure DMSO, methanol, and ethanol with HRS spectra and depolarization ratios compared against existing literature. Other additional data including comparisons of HRS features against IR and Raman in literature and UV absorption cross-sections for the solutions studied. See DOI: 10.1039/x0xx00000x

Hyper-Rayleigh and hyper-Raman spectra for the biomolecules discussed in the article and ESI have been deposited in numerical form at the Texas Data Repository at [INSERT URL AFTER ACCEPTANCE https://doi.org/DOI].

Acknowledgements

The authors received partial funding from the National Science Foundation (NSF) (DBI-1455671, ECCS-1509268, CMMI-1826078), the Air Force Office of Scientific Research (AFOSR) (FA9550-15-1-0517, FA9550-20-1-0366, FA9550-20-1-0367), Army Medical Research Grant (W81XWH2010777), the National

Institutes of Health (NIH) (1R01GM127696-01, 1R21GM142107-01), the Cancer Prevention and Research Institute of Texas (CPRIT) (RP180588). E. Keene was supported by the Texas A&M University (TAMU) Undergraduate Summer Research Grant Program. C. Marble is supported by the TAMU GREAT Program. C. Marble and K. Marble are supported by the NSF Graduate Research Fellowship Program (NSF GRFP). This material is based upon work supported by the NSF GRPF under Grant No. DGE 1746932. Any opinions, findings, and conclusions or recommendations expressed in this material are those of the authors and do not necessarily reflect the views of the National Science Foundation.

References

1 R. Bhattacharjee, Y. S. Jain, and H. D. Bist, *J. Raman Spectroscopy,* 1989, **20**(2), 91-97.
2 M. T. Rosado, M. L. R. S. Duarte, and R. Fausto, *J. Molecular Structure*, 1997**, 410-411**, 343-348.
3 J. J. Max and C. Chapados, J. Physical Chemistry A, 2001, **105**(47), 10681-10688.
4 S. Kumar, A. K. Rai, S. B. Rai, D. K. Rai, A. N. Singh, and V. B. Singh, J. *Molecular Structure*, 2006, **791**, 23-29.
5 B. Z. Chowdhry, T. J. Dines, S. Jabeen, and R. Withnall, *J. Physical Chemistry A*, 2008, **112**(41), 10333-10347.
6 E. Wiercigroch, E. Szafraniec, K. Czamara, M. Z. Pacia, K. Majzner, K. Kochan, A. Kaczor, M. Baranska, and K. Malek, *Spectrochimica Acta - Part A: Molecular and Biomolecular Spectroscopy,* 2017, **185**, 317-335.
7 K. B. Beć, J. Grabska, and C. W. Huck, *Molecules*, 2020, **25**(12), 2948.
8 J. de Gelder, K. de Gussem, P. Vandenabeele, and L. Moens, *J. Raman Spectroscopy,* 2007, **38**(9), 1133-1147.
9 A. M. Kelley, L. C. T. Shoute, M. Blanchard-Desce, G. P. Bartholomew, and G. C. Bazan, *Molecular Physics,* 2006, **104**(8), 1239-1247.
10 Q. Xu, Y. Liu, M. Wang, J. Cerezo, R. Improta, and F. Santoro, *Molecules*, 2023, **28**(5), 2286.
11 X. X. Han R. S. Rodriguez, C. L. Haynes, Y. Ozaki, and B. Zhao*, Nat. Rev. Methods Primers,* 2021, **1**(87), 1-17.
12 G. I. Petrov, V. V. Yakovlev, A. V. Sokolov, and M. O. Scully, *Optics Express,* 2005, **13**(23), 9537-9542.
13 A. D. Shutov, J. T. Harrington, H. Zhu, D. W. Wang, D. Zhang and V. V. Yakovlev, *IEEE Journal of Selected Topics in Quantum Electronics,* 2021, **27**(5)**, 1-6.**
14 G. I. Petrov, R. Arora, and V. V. Yakovlev, *Analyst*, 2021, **146**, 1253-1259.
15 C. Zong, R. Premasiri, H. Lin, Y. Huang, C. Zhang, C. Yang, B. Ren, L. D. Ziegler, and J. Cheng, *Nature Communications,* 2019, **10**, 5318.
16 Y. Shingaya, H. Takaki, N. Kobayashi, M. Aono, and T. Nakayama, *Nanoscale.* 2022, **14**, 14552-14557.
17 K. Rahmelow and W. Hübner, *Applied Spectroscopy,* 1997, **51**(2), 160-170.
18 D. L. Andrews and T. Thirunamachandran, *The J. Chemical Physics,* 1979, **70**(2), 1027-1030.
19 C. C. Bonang, S. M. Cameron, J. D. Getty, and P. B. Kelly, *Chemical Physics Letters,* 1993, **209**(1), 35-41.
20 M. Okuno, Journal of Chemical Physics, 2020, **152**(17), 174202.
21 X. Xu. C. B. Marble, G. I. Petrov, D. Wang, and V. V. Yakovlev, Proc. SPIE 11252, *Proc. SPIE 11252, Advanced Chemical Microscopy for Life Science and Translational Medicine*, 112521T, 2020**.**
22 C. B. Marble, X. Xu, K. S. Marble, G. I. Petrov, D. Wang, and V. V. Yakovlev, Proc. SPIE 11252, Advanced Chemical Microscopy for Life Science and Translational Medicine, 112520V. 2020.
23 C. B. Marble, X. Xu, M. Keppler, E. Gil, G. I. Petrov, D. Wang, and V. V. Yakovlev, *Proc. SPIE 11288, Quantum Sensing and Nano Electronics and Photonics XVII,* 1128829, 2020.
24 F. Chen and S. Mukamel, *ACS Photonic,* 2021, 8(9), 2722-2727.
25 M. Asakura and M. Okuno, *J. Physical Chemistry Letters*, 2021, **12**(20), 4780-4785.
26 C. B. Marble, X. Xu, G. I. Petrov, D. Wang, and V. V. Yakovlev, Proc. SPIE 11656, Advanced Chemical Microscopy for Life Science and Translational Medicine, 116560C, 2021.
27 C. B. Marble, X. Xu, G. I. Petrov, D. Wang, and V. V. Yakovlev, *Phys. Chem. Chem. Phys,* 2021, **23**, 24047-24051.
28 K. Inoue and M. Okuno, J. Raman Spectroscopy, 2022, **53**(10), 1679-1685.
29 S. J. Cyvin, J. E. Rauch, and J. C. Decius, *The J. Chemical Physics*, 1965, **43**(11), 4083-4095.
30 Y. C. Chung and L. D. Ziegler, *The J. Chemical Physics,* 1988, **88**(12), 7287-7294.
31 S. Kielich and T. Bancewicz, *Journal of Raman Spectroscopy*, 1990, ***21***(12), 791-796.
32 A. M. Kelley, *Annu. Rev. Phys. Chem.* 2010, **61**, 41−61.
33 K. A. Forbes, *J. Opt.*, 2020, **22**(9), 095401.
34 R. Tan, D. F. Kelley, and A. M. Kelley, *J. Phys. Chem. C,* 2019, **123**, 16400–16405.
35 C. N. Yu and H. Hiramatsu, *Journal of the Chinese Chemical Society*, 2022, **69**(1), 60-65.
36 J. T. Golab, J. R. Sprague, K. T. Carron, G. C. Schatz, and R. P. van Duyne, *The J. Chemical Physics*, 1988, **88**(12)*,* 7942-7951.
37 K. Inoue, T. Morimoto, D. Yokogawa, and M. Okuno, *J. Chemical Physics*, 2022, **157**(5), 054505.
38 C. C. Yu, K. Y. Chiang, M. Okuno, T. Seki, T. Ohto, X. Yu, V. Korepanov, H. O. Hamaguchi, M. Bonn, J. Hunger, and Y. Nagata, *Nat. Commun*, 2020, **11**(1), 5977.
39 V. Korepanov, C. C. Yu, and H. Hamaguchi, *J. Raman Spectroscopy,* 2022, **53**(10), 1666-1668.
40 K. Inoue, Y. Litman, D. M. Wilkins, Y. Nagata, and M. Okuno, *J. Phys. Chem. Lett.,* 2023, **14**(12), 3063–3068.
41 C. Wen, C. Yu, N. Thirumalaivasan, and H. Hiramatsu, *J. Raman Spectroscopy*, 2020, **52**(3), 641-654.
42 C. I. Wen and H. Hiramatsu, *J. Raman Spectroscopy.* 2020**,** **51**(2), 274-278.
43 M. Okuno, *J. Raman Spectroscopy*, 2021, **52**(4), 849-856.
44 Y. Ukaji and T. Soeta, *Comprehensive Chirality*, 2012, **3**, 176-201.
45 E. R. Alonso, I. León, L. Kolesniková, S. Mata, and J. L. Alonso, *Angewandte Chemie - International Edition*, 2021, **60**(32), 17410-17414.
46 P. L. Polavarapu, J. L. Johnson, V. Raghavan, G. Zając, G., and M. Baranska, *J. Raman Spectroscopy*, 2022, **53**(6), 1102-1114.
47 S. Maity and H. Hiramatsu, *J. Raman Spectroscopy*, 2022, **53**(11), 1845-1847.
48 L. Hao, X. Lu, M. Sun, K. Li, L. Shen, and T. Wu, *Food and Nutrition Research*, 2015, **59**, 1-10.
49 K. Pol, K. de Graaf, M. D. Bruin, M. Balvers, and M. Mars, *J. Functional Foods*, 2020, **73**, 104114.
50 H. Li, R. Ding, Y. Shan, F. Ye, Y. Lin, X. Men, C. Chen, S. Tan, Q. Wang, and B. Hu, *J. Functional Foods*, 2021, **87**, 104839.
51 J. Reader, C. J. Sansonetti, and J. M. Bridges, *Applied Optics,* 1996, **35**(1), 78-83.
52 M. D. Dauchez, P. Derreumaux, and G. Vergoten, *The Journal of Compound Chemistry*, 1992, **14**(3), 263-277
53 M. B. Marry, V. Sasirekha, and V. Ramakrishnan, *Spectrochimica Acta Part A,* 2006, **65** (2), 414-420
54 L. D. Barron, A. R. Gargaro, and L. Hecht, *Spectrochimica Acta Part A,* 1992, **48**(8), 1051-1066
55 M. Lettieri, *Vibrational Spectroscopy*, 2015, **76**, 48-54.

